

1 **Title: Selective targeting of striatal parvalbumin-expressing interneurons for**
2 **transgene delivery.**

3 Marcelo Duarte Azevedo^{1,§}, Sibilla Sander^{1,§}, Cheryl Jeanneret¹, Soophie Olfat^{1,#}, Liliane
4 Tenenbaum^{1,*}.

5 ¹Laboratory of Neurotherapies and NeuroModulation, Center for Neuroscience Research,
6 Clinical Neurosciences Department, Lausanne University Hospital, Switzerland.
7

8

9

10 **Highlights**

- 11 • Cre recombinase decreases the number of striatal but not cortical PV⁺ interneurons.
12 • Viral vector diffusion hinders striatal selective transgene delivery in PV^{Cre} mice.
13 • Weak retrograde transduction of PV⁺ pallidostriatal projection neurons.
14

15 **Keywords**

- 16 • Parvalbumin, fast-spiking interneurons, striatum, PV^{Cre} mice, AAV-FLEX vectors
17
18

19 §Both authors equally contributed to this work

20 #Present address: Division of Neurogeriatrics, Department of Neurobiology, Care Sciences and
21 Society (NVS), Karolinska Institutet, Sweden

22 *Corresponding author: Liliane.Tenenbaum@chuv.ch
23

24

25 **Abstract**

26 PV^{Cre} mice combined with AAV-FLEX vectors allowed efficient and specific targeting of PV⁺
27 interneurons in the striatum. However, diffusion of viral particles to the globus pallidus
28 caused massive transduction of PV⁺ projection neurons and subsequent anterograde
29 transport of the transgene product to the subthalamic nucleus and the substantia nigra pars
30 reticulata.

31 Different AAV serotypes (1 and 9) and promoters (CBA and human synapsin) were
32 evaluated. The combination of AAV1, a moderate expression level (human synapsin
33 promoter) and a precise adjustment of the stereotaxic coordinates in the anterior and
34 dorsolateral part of the striatum were necessary to avoid transduction of PV⁺ GP projection
35 neurons.

36 Even in the absence of direct transduction due to diffusion of viral particles, GP PV⁺
37 projection neurons could be retrogradely transduced via their terminals present in the dorsal
38 striatum. However, in the absence of diffusion, GP-Str PV⁺ projection neurons were poorly or
39 not transduced suggesting that retrograde transduction did not significantly impair the
40 selective targeting of striatal PV⁺ neurons.

41 Finally, a prominent reduction of the number of striatal PV⁺ interneurons (about 50%) was
42 evidenced in the presence of the Cre recombinase suggesting that functional effects of AAV-
43 mediated transgene expression in PV⁺ striatal interneurons in PV^{Cre} mice should be analyzed
44 with caution.

45

46 **Introduction**

47 AAV vectors have gained increasing interest for gene therapy of neurological diseases
48 (Kantor, McCown et al. 2014) (Hocquemiller, Giersch et al. 2016) as well as for functional
49 studies in neuroscience research (Bedbrook, Deverman et al. 2018). Targeting specific
50 neuronal subpopulations is a rapidly growing field allowing the manipulation of neuronal
51 circuits using optogenetics (Hunnicut, Jongbloets et al. 2016) or chemogenetics

52 (Woloszynowska-Fraser, Wulff et al. 2017), the modeling of disease using human disease-
53 causing transgenes (Grames, Dayton et al. 2018) as well as next-generation targeted gene
54 therapy (Chtarto, Bockstael et al. 2013) (Dalkara, Byrne et al. 2013) (Vormstein-Schneider,
55 Lin et al. 2020). Thanks to their ability to be axonally transported (Castle, Gershenson et al.
56 2014), AAV vectors are also useful for anatomical tracing (Zingg, Chou et al. 2017).

57 The cell-type specificity of AAV-mediated transgene expression is dependent on the viral
58 capsid and the regulatory elements driving transcription. Numerous vectors selectively
59 targeting neurons or glial cells have been described. Selective gene expression into neurons
60 can be achieved using pan-neuronal promoters such as the neuron-specific enolase (Klein,
61 Meyer et al. 1998, Klein, Hamby et al. 2002) or the synapsin (Kugler, Lingor et al. 2003,
62 Shevtsova, Malik et al. 2005) (Dashkoff, Lerner et al. 2016) (Nieuwenhuis, Haenzi et al.
63 2020) promoters. Specific targeting of excitatory neurons has been described using the
64 calmodulin kinase II (CaMKII α) promoter (Kim, Kim et al. 2015, Watakabe, Ohtsuka et al.
65 2015). Oligodendrocytes have been targeted using the myelin-basic protein promoter (Chen,
66 McCarty et al. 1998, Chen, McCarty et al. 1999), astrocytes using assembled fragments of
67 the glial fibrillary protein promoter (GFA) (Drinkut, Tereshchenko et al. 2012) (Meunier,
68 Merienne et al. 2016) (Pignataro, Sucunza et al. 2017) (Dashkoff, Lerner et al. 2016)
69 (Dashkoff, Lerner et al. 2016) and microglia using the F4/80 or the CD68 promoter (Rosario,
70 Cruz et al. 2016). In some cases, the cellular specificity is obtained independently of the
71 chosen capsid. For example, the GFA promoter drives expression mainly in astrocytes,
72 when combined with AAV5 (Drinkut, Tereshchenko et al. 2012), AAV6 (Dirren, Towne et al.
73 2014) AAV8 (Pignataro, Sucunza et al. 2017), AAV9 (Dashkoff, Lerner et al. 2016) or AAV-
74 D/J capsids (Jolle, Deglon et al. 2019). In contrast, the combination of a cell type-specific
75 promoter and a capsid variant was necessary to transduce microglial cells (Rosario, Cruz et
76 al. 2016). Finally, brain endothelial cell-specific targeting was obtained using a novel capsid
77 variant combined with a non-specific promoter (chicken β -actin promoter fused to
78 cytomegalovirus enhancer sites) (Korbelin, Dogbevia et al. 2016).

79 The development of vectors selectively targeting neuronal subpopulations is coming of
80 age. Some examples are: GluA4-AAV a capsid variant designed to attach to glutamate
81 receptor 4 (GluA4), selectively expressed by parvalbumin-positive (PV+) interneurons
82 (Geiger, Melcher et al. 1995), combined with the SFFV (spleen focus-forming virus)
83 promoter (Hartmann, Thalheimer et al. 2019); AAV-mDlx a vector targeting interneurons
84 using mDlx transcriptional regulatory elements combined with AAV9 (Dimidschstein, Chen et
85 al. 2016) or AAV5 (Lee, Vogt et al. 2014) capsids; AAV-TH which is targeting dopaminergic
86 neurons thanks to the use of a fragment of the tyrosine hydroxylase promoter (Stauffer, Lak
87 et al. 2016) and AAV PHP.eB with hybrid promoters containing specific enhancers targeting
88 PV- and VIP- interneurons (Vormstein-Schneider, Lin et al. 2020).

89 With the advent of single-cell RNA sequencing (Munoz-Manchado, Bengtsson Gonzales
90 et al. 2018) (Gokce, Stanley et al. 2016) and methods for mapping chromatin accessibility
91 (Buenrostro, Wu et al. 2015), new synthetic promoters will eventually be identified, which will
92 further refine these molecular tools (Juttner, Szabo et al. 2019).

93 Targeting specific neuronal subpopulations can also be achieved using a combination of
94 Cre-driver mice (Hippenmeyer, Vrieseling et al. 2005) or rats (Liu, Brown et al. 2016)
95 expressing the Cre recombinase under the control of a cell-type specific gene and an AAV
96 vector harboring an inverted ORF flanked by 2 pairs of Cre recognition sites positioned so
97 that expression occurs only when the Cre protein is present (Saunders, Johnson et al. 2012,
98 Saunders and Sabatini 2015).

99 In the striatum, projection neurons, also called medium-sized spiny neurons, relay motor
100 output, expressing D1R- or D2R-type of dopamine receptors which, in response to dopamine
101 respectively activate (D1R) or inhibit (D2R) efferent structures of the motor loop (Surmeier,
102 Ding et al. 2007). The striatum also contains several classes of interneurons among which
103 the (PV+) fast spiking and the cholinergic neurons which are thought to coordinate the
104 activity of the projection neurons (Gritton, Howe et al. 2019).

105 In the present study, we have focused on the targeting of PV+ interneurons of the dorso-
106 lateral striatum which are key to the control of the sensorimotor striatum (Lee, Holley et al.
107 2017) using PV^{Cre} driver mice (Hippenmeyer, Vrieseling et al. 2005).

108 Limitations of the AAV-FLEX/Cre driver mice targeting system have been previously
109 described: i) off-target expression in cells not expressing Cre (Fischer, Collins et al. 2019), ii)
110 expression of Cre in only a part of the targeted neuronal population (Saunders, Huang et al.
111 2016), iii) Cre recombinase-induced cellular abnormalities (He, Marioutina et al. 2014).

112 We show here that, despite the efficient and specific cellular targeting offered by the Cre-
113 lox system, the AAV delivery parameters have to be precisely adjusted to selectively target
114 the striatum with exclusion of the adjacent globus pallidus containing a high density of PV+
115 projection neurons. Furthermore, PV⁺ striatal interneurons were decreased by the Cre-
116 recombinase. These data suggest that functional effects of AAV-FLEX transgene expression
117 in PV⁺ striatal interneurons in PV^{Cre} mice should be analyzed with caution.

118

119 **Material and Methods**

120 *Animals*

121 Pvalbm1(Cre)Arbr (PV^{Cre}) mice (www.jax.org: 008069) (Hippenmeyer, Vrieseling et al. 2005)
122 in which a IRES-Cre-polyA cassette was introduced in the 3'UTR region of exon 5 of the PV
123 gene, were genotyped using the following primers: Cre-forward, 5' GCG GTC TGG CAG
124 TAA AAA CTA TC 3'; Cre-reverse, 5' GTG AAA CAG CAT TGC TGT CAC TT 3'; PVexon5
125 forward, 5' CAG AGC AGG CAT GGT GAC TA 3'; PVexon5 reverse, 5' CCA TTC GCC ATT
126 AGT CTG GT 3. PCR conditions were: 4 min at 94°C followed by 25 cycles of 94°C for 30
127 sec, 60°C for 1 min, 72°C for 1 min.

128 Eleven weeks-old homozygous PV^{Cre} mice and wild-type (WT) C57Bl6-Ola-Hsd mice (En
129 Vigo) of both sexes were used for all experiments.

130

131 *Plasmids*

132 AAV pCAG-FLEX-eGFP-WPRE (Plasmid #51502) and AAV phSyn1(S)-FLEX-eGFP-WPRE
133 (Plasmid #51504) (Oh, Harris et al. 2014) were obtained from AddGene
134 (<http://www.addgene.org>).

135 pAAV2/1 and pAAV2/9 were provided by the Penn Vector Core (Philadelphia,
136 Pennsylvania). pAd-helper was purchased from Stratagene (La Jolla, California),

137

138 *AAV production*

139 The 3 viruses used in this study were produced by triple transfection of HEK-293T cells (30
140 (10cm) plates; 5.0×10^6 cells per plate). The AAV helper plasmids; pAAV2/1 or pAAV2/9,
141 expressing the AAV viral genes, were co-transfected with an adeno-helper plasmid (pAd-
142 helper), expressing the adenoviral genes required for AAV replication and encapsidation
143 together with the vector plasmids; AAV-phSyn1- FLEX -eGFP-WPRE or AAV-pCAG-FLEX-
144 eGFP-WPRE in a 2:3:5 molar ratio. Fifty hours post-transfection, cells were harvested by
145 low-speed centrifugation, medium was discarded, and cells were resuspended in Tris 50 mM
146 pH 8.5, NaCl 0.1M, EDTA 1mM and kept at -20°C. After five freezing/thawing cycles at -
147 20°C/37°C, the cell lysate was centrifuged 20 min at 11,000 rpm. The supernatant was
148 recovered and treated with benzonase (50 units/ml, Sigma) for 30 min at 37°C and
149 centrifuged again 20 min at 11,000 rpm to eliminate residual debris. The viruses were further
150 purified by iodixanol gradient and microconcentrated as described previously (Zolotukhin,
151 Potter et al. 2002).

152 Viral genomes (vg) were titrated by quantitative polymerase chain reaction using universal
153 primers located in the viral ITR sequence as previously described (Aurnhammer, Haase et
154 al. 2012). Titers were 1.72×10^{14} vg/ml for AAV1-hsyn- FLEX -eGFP, 1.03×10^{14} vg/ml for
155 AAV9-hsyn- FLEX -eGFP and 5.24×10^{13} vg/ml for AAV9-CBA- FLEX -eGFP.

156

157 *Stereotaxic injections*

158 Adult mice (11 weeks-old) were used for unilateral intrastriatal injections. Briefly, the animals
159 were anesthetized with a mixture of ketamine (100 mg/kg, Ketazol, Graeb AG) and xylazine

160 (10 mg/kg, Rompun, Bayer). Injections were made according to coordinates defined by “The
161 Mouse Brain in stereotaxic coordinates, 3rd edition, Franklin, K.B.J. and Paxinos, G.
162 AcademicPress, 2007” using a Kopf stereotaxic apparatus (David Kopf, Tujunga, California).
163 Viral particles diluted in 1 µl of D-PBS (Biowhittaker, Lonza) were infused in the striatum,
164 using a 34G needle at different coordinates (see Table 1). After injection, the needle was left
165 in place for 5 min in order to allow diffusion of the viral suspension in the parenchyma. The
166 needle was then slowly removed. Animals were maintained in a 12:12 hrs light-dark cycle
167 with free access to food and water.

168 Experimental procedures were approved by the “Affaires vétérinaires” of the Canton de
169 Vaud” (Authorization n°VD3400).

170

171 *Brain collection and immunohistochemistry*

172 Two weeks after viral injection, mice were euthanized with an overdose of pentobarbital (30
173 mg/kg in 0.9% NaCl). A 4% paraformaldehyde (PFA) solution at pH 7.4 in phosphate buffer
174 saline (PBS, Bichsel AG) was freshly prepared before use. The mice were transcardially
175 perfused consecutively with a PBS solution at pH 7.4 and with the ice-cold 4% PFA solution.
176 Brains were collected and post-fixed in 4% PFA overnight at 4°C. Consecutive incubations
177 of 24h in 20% and 30% sucrose solutions were performed to cryoprotect the brains which
178 were then slowly frozen by consecutive immersions in 2-methyl-butane at -10°C and -20°C
179 and finally stored at -80°C. A cryostat (Leica Biosystems, CM1850) was used to collect
180 25µm-thick coronal sections which were stored in an anti-freeze solution (glycerol 25%,
181 ethylene glycol 30% and Na-phosphate buffer 50mM) at -20°C. The following antibodies
182 were used to stain PV+ cells: guinea pig anti-PV (1:1000, cat. #195004, Synaptic Systems,
183 Göttingen, Germany), biotinylated goat anti-guinea pig (1:200, cat. #BA-7000, Vector
184 Laboratories, Burlingame, USA) and Cy3-conjugated streptavidin (1:300, cat. #016-160-084,
185 Jackson ImmunoResearch Laboratories, West Grove – USA). Free floating sections were
186 stained as follows. Sections were washed 3 times for 10 min in Tris-buffered saline (TBS,
187 10mM Tris pH 7.6 and 0.9% NaCl) at room temperature (RT). Then, they were incubated 1h

188 at RT in a blocking solution composed of 5% bovine serum albumin (BSA) in THST buffer
189 (50mM Tris pH 7.6, 0.5M NaCl and Triton X-RT100 0.5%). Afterwards, they were incubated
190 overnight at 4°C with the primary antibody in a THST solution containing 1% BSA. The
191 second day, sections were first washed 3 times for 10 min in TBS at RT and then incubated
192 for 1h at RT with the secondary antibody in THST. Sections were then washed 3 times for 10
193 min in TBS and incubated in the dark with the streptavidin conjugate for 1h at RT in THST.
194 Finally, the sections were washed 3 times in PBS for 10 min at RT. The sections were
195 mounted on microscope slides and covered with Vectashield mounting medium (Vector
196 Laboratories, Burlingame, USA).

197

198 *Image acquisition and quantifications*

199 Whole slide images were taken with a Zeiss Axioscan Z.1 slide-scanner (Carl Zeiss
200 Microscopy, Germany) using a Plan-Apochromat 10x/0.45 or a Plan-Apochromat 20x/0.8
201 objective. All the images were taken with an Orca-Flash 4.0 V2 digital CMOS camera. 16
202 bits images were obtained. Cy3 was excited at 553 nm with a 555/30 nm LED at 50% power.
203 A beam splitter at 568nm was used. The detection range was 578-640nm. eGFP was
204 excited at 493nm with a 469/38 nm LED at 20% of power. A beam splitter at 498 was used.
205 Detection range was 507-546nm. Confocal images were taken with a confocal microscope
206 Zeiss LSM 800 (Carl Zeiss Microscopy, Germany) equipped with a 3x GaAsp detector. All
207 images were collected with a Plan Apochromat 20x / 0.8 DIC II objective with a pinhole set at
208 36 µm. 8 bits resolution images have been obtained by bidirectional scanning and 4x
209 averaging. Cy3 was excited with a 561 nm laser at 0.03% of power. 739V of master gain
210 was applied and the detection range was 566-628 nm. eGFP was excited with a 488nm
211 laser at 0.03% of power. 750V of master gain was applied and the detection range was 410-
212 546 nm. Controls with single-fluorescence were performed. No interference between red and
213 green fluorescence was observed.

214 Images were processed using Zen Blue 2.3 (Carl Zeiss Microscopy, Germany) and
215 ImageJ/Fiji. Z-stacks were acquired on a 25 μm thickness. Shown confocal images in Fig. 1,
216 2,5 and 6, are 2D maximal intensity projections of 35 images. .

217 Cells were manually counted on 2D maximal intensity projections of confocal images
218 transformed into the tiff format. Cells were counted by a blind observer using the Multi-point
219 tool in ImageJ. For evaluating the specificity, GFP⁺, PV⁺, and double-labeled cells were
220 counted. For each animal, five brain sections were selected, and three pictures were taken
221 for each section. To evaluate the efficacy in the dorsal striatum, the striatum was divided in
222 two by a horizontal line, and GFP⁺, PV⁺, and double-labeled cells were counted in the upper
223 part.

224 For the quantification of native GFP fluorescence intensity of individual cells (Fig. 6),
225 confocal images were used and the cells were delineated using the “free-hand” selection tool
226 of the ImageJ software. The mean fluorescence intensity was recorded for each individual
227 cell. Area with a similar surface in non-transduced area of the GP or striatum were measured
228 and the obtained values subtracted.-

229 In order to evaluate Cre recombinase effect on PV⁺ cells, WT and PV^{Cre} mice were
230 compared. For each AAV-FLEX virus, three WT and three PV^{Cre} successfully injected
231 animals were available. The number of PV⁺ cells in the non-injected hemisphere was
232 counted on a section from the same region for each animal and divided by the surface in
233 mm^2 . The images were transformed in .jpeg format at a resolution of 300dpi and countings
234 were performed by a blind observer using the Multi-point tool in ImageJ.

235 To determine viral toxicity the number of PV⁺ cells of the injected hemisphere was compared
236 to the corresponding area in the non-injected hemisphere. In order to count cells in the
237 whole striatum, images were acquired with the slide scanner. The images were transformed
238 in .jpeg at a resolution of 300dpi format and cells were counted by a blind observer using the
239 Multi-point tool in ImageJ.

240

241 *Statistical analysis*

242 Data analyses and the creation of graphs were performed using GraphPad Prism 8 software
243 (San Diego, CA) for Windows. Comparisons were performed by One-way ANOVA followed
244 by Tukey's multiple comparisons test (Table 2), two-way ANOVA followed by Sidak post hoc
245 test (for more than 2 groups) or by Student t-test (2 groups). Results were expressed as
246 mean \pm SD and statistical significance was established for a p value \leq 0.05.

247

248

249 **Results**

250 *Efficiency and cellular specificity of transgene expression in striatal PV⁺ interneurons*
251 *mediated by AAV2/9-FLEX vectors in PV^{Cre} mice.*

252 AAV-FLEX vectors and PV^{Cre} mice were used to target transgene expression into striatal
253 PV⁺ interneurons. Since PV expression was weaker in the striatum than in other brain
254 regions (for example in the cerebral cortex; see Suppl. Fig. 1), we used AAV-FLEX vectors
255 (Oh, Harris et al. 2014) with strong promoters; the non-specific CMV/chicken β -actin (CBA)
256 promoter (Burger, Gorbatyuk et al. 2004) (Klein, Hamby et al. 2002) or the neuron-specific
257 human synapsin promoter (hsyn) (Shevtsova, Malik et al. 2005) combined with the
258 "Woodchuck hepatitis virus post-transcriptional regulatory element" (WPRE) which enhances
259 mRNA stability and protein synthesis (Klein, Hamby et al. 2002) (Oh, Harris et al. 2014). In
260 order to further maximize transduction efficiency, the vectors were encapsidated into AAV9
261 serotype (Cearley and Wolfe 2006) (Klein, Dayton et al. 2008).

262 The vectors (7.9×10^9 vg in 1 μ l) were injected in the striatum of homozygous PV^{Cre} mice
263 using various coordinates (see Table 1). As a negative control, the vectors were also

264 injected in WT C57/Bl6 mice.

Virus	Coordinates (AP, ML, DV)	Total number of animals	Number of animals with a GP transduction
AAV2/9-CBA-FLEX-eGFP	+1.1, -1.8, -3.0	1	0
	+1.2, -1.8, -3.0	3	2
AAV2/9-hsyn-FLEX-eGFP	+1.0, -1.8, -3.0	3	3
	+1.1, -1.8, -3.0	3	1
	+1.2, -1.8, -3.0	3	2
	+1.2, -1.8, -2.75	3	2
AAV2/1-hsyn-FLEX-eGFP	+1.0, -1.8, -3.0	2	1
	+1.2, -1.8, -2.75	3 + 4*	0

265

266 **Table 1: Summary of the coordinates sets and of the number of animals used for each**
 267 **AAV-FLEX virus.**

AP: antero-posterior, ML: mediol-lateral, DV: dorso-ventral, GP: globus pallidus.

*These 4 mice were not included in the analysis of the efficiency and specificity of AAV2/1-hsyn-FLEX-eGFP vector due to a drastic loss of PV-expressing striatal cells in this littermate precluding statistical analysis (see below and Suppl. Fig.2).

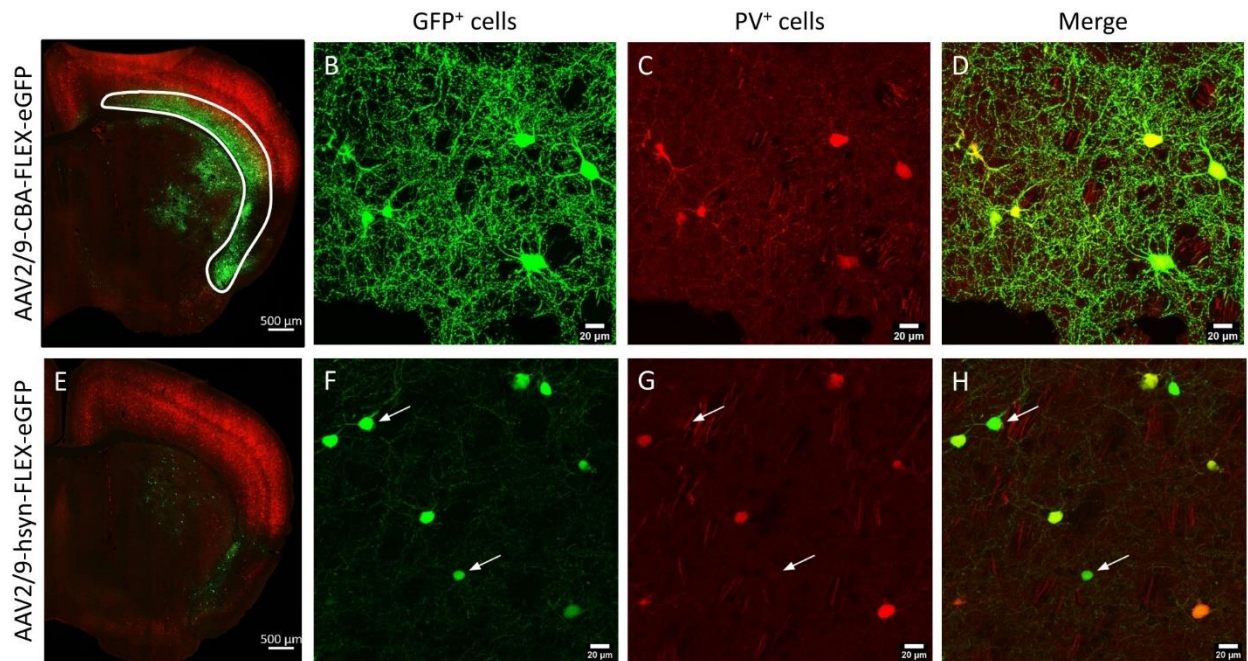
268

269 GFP⁺ cells were observed in the striatum with a distribution corresponding to the expected
 270 pattern of PV⁺ interneurons (Fig.1 A & E). GFP⁺ fibers were more strongly labeled with the
 271 CBA promoter (Fig.1 B & D) as compared with the hsyn promoter (Fig.1 F & H), suggesting,
 272 that, as expected, the hybrid (cellular/viral) CBA promoter drives a higher transgene
 273 expression level than the cellular hsyn promoter.

274 In order to confirm the cell-type specificity of transgene expression, brain sections were
 275 labeled with anti-PV antibodies.

276 The efficiency of PV⁺ interneurons transduction, evaluated as the number of double-labeled
 277 PV⁺/GFP⁺ cells (Fig.1 D & H), relative to the total number of PV⁺ cells (Fig.1 C & G) was
 278 similar (>90%) for both promoters in AAV2/9 vectors (n=5 for hsyn and n=3 for CBA) (Table
 279 2). The specificity of the targeting, evaluated as the number of double-labeled PV⁺/GFP⁺
 280 cells relative to the total number of GFP⁺ cells (Fig.1 B & F), was approx. 85-90% for both
 281 promoters (Table 2). Few GFP⁺ cells which did not show a detectable PV staining were
 282 observed (Fig.1, arrow), suggesting that a low level of non-specific expression could have
 283 occurred. However, injection into WT C57/Bl6 mice did not reveal any GFP⁺ cell (data not
 284 shown), suggesting that, as expected GFP expression was dependent on the presence of

285 the Cre recombinase. The GFP⁺ cells which were not labeled by anti-PV antibodies could be
 286 due to a low, undetectable PV expression in these neurons or to a potential toxicity of the
 287 Cre recombinase (see below).



288

289 **Figure 1. Efficiency and specificity of AAV2/9-FLEX-mediated PV⁺ striatal interneurons**
 290 **transduction in PV^{Cre} (+/+) mice**

PV^{Cre} (+/+) mice were injected with AAV2/9-CBA-FLEX-eGFP (A,B,C,D) or AAV2/9-hsyn-FLEX-eGFP (E,F,G,H) vectors. A & E, Distribution of GFP⁺ cells in the striatum (Axioscan 20-fold). Confocal pictures showing co-localization (D,H) of native GFP fluorescence (B,F) with parvalbumin staining (C,G). Arrows show cells expressing GFP but without detectable PV staining. Panel A surrounded area: transduced area in the cortex. Control wild-type mice injected with the same vectors did not harbor GFP⁺ cells (data not shown).

291

Virus	Efficiency Double GFP ⁺ /PV ⁺ among total PV ⁺ (%) (Mean ± SD)	Specificity Double GFP ⁺ /PV ⁺ among total GFP ⁺ (%) (Mean ± SD)
AAV2/9-CBA-FLEX-eGFP	94.85 ± 3.36	88.69 ± 3.22
AAV2/9-hsyn-FLEX-eGFP	99.49 ± 0.88	84.97 ± 3.56
AAV2/1-hsyn-FLEX-eGFP	93.48 ± 1.72	89.21 ± 2.20

292

293 **Table 2: Percentage of PV/GFP double-labeled cells among total GFP⁺ cells**
 294 **(specificity) or total PV⁺ cells (efficiency) in the dorsal striatum**

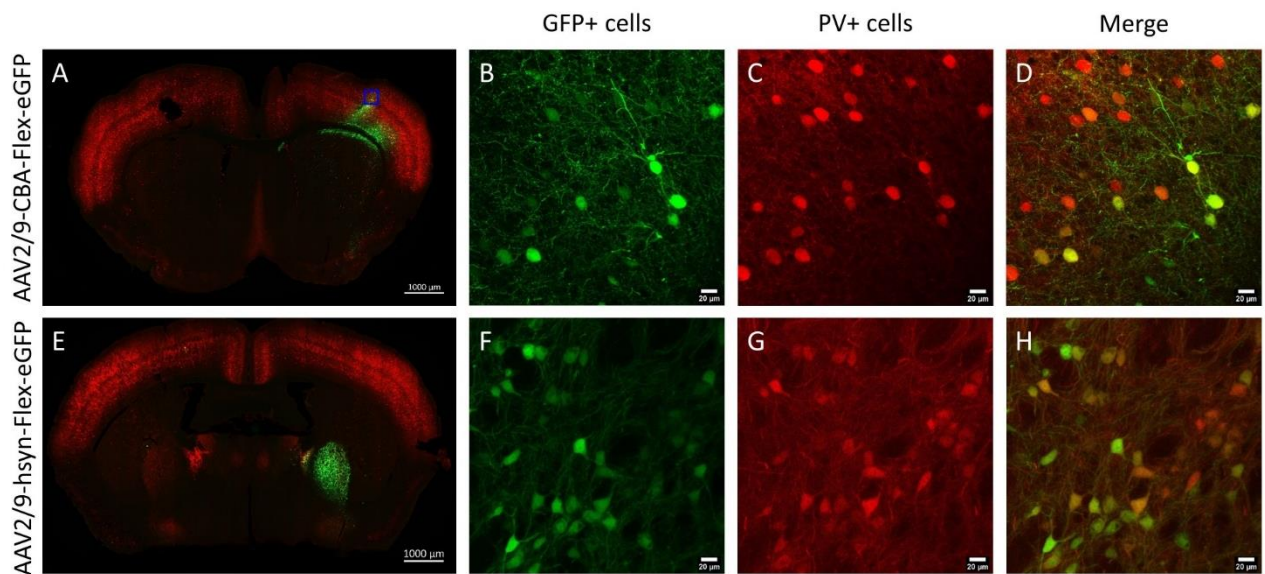
295 Data were analyzed using one-way ANOVA followed by Tukey's multiple comparisons test. Difference
 296 between vectors were not significant for specificity. For efficiency, AAV2/1-hsyn-FLEX-eGFP was
 297 significantly lower than AAV2/9-hsyn-FLEX-eGFP (p=0.0380)

298

299 *Transduction of contiguous and axonally-connected brain regions*

300 Examination of the whole brains revealed GFP⁺ cells in the globus pallidus (GP) (Fig. 2E)
301 and in the cerebral cortex (CTX) (Fig. 2A) in a large proportion of the animals. These data
302 suggest that viral particles diffused to these neighboring regions which contain a higher
303 density of PV⁺ neurons as compared to the striatum (Saunders, Huang et al. 2016).
304 The localized cortical transduction was probably due to a reflux of the viral suspension along
305 the needle and could be avoid using anti-reflux needles (Vazquez, Hagel et al. 2012,
306 Casanova, Carney et al. 2014, Lueshen, Tangen et al. 2017).
307 The majority of GFP⁺ cells also expressed PV in the cerebral cortex (Fig. 2 B-D) as well as in
308 the GP (Fig.2 F-H).
309 Preferential transduction of the GP after injection of AAV vectors in the striatum has been
310 previously reported (Tenenbaum, Jurysta et al. 2000) and was suggested to reflect a
311 preferential diffusion of the viral particles along the vessels driven by the perivascular pump
312 (Hadaczek, Yamashita et al. 2006).
313 Several stereotaxic coordinates were tested in order to reduce diffusion to extra-striatal
314 areas (see Table 1). The anteroposterior coordinate varied between +1.0 and +1.2, the
315 dorsoventral coordinate varied between -2.75 and -3.0 and mediolateral coordinate was set
316 at -1.8. For both promoters, the majority of the mice harbored a widespread transduction of
317 the GP (see Table 1). With none of the coordinates was the GP transduction avoid in all

318 mice.



319

320 **Figure 2: Efficient transduction of PV⁺ neurons in globus pallidus and cerebral cortex.**

PV^{Cre} (+/+) mice were injected with AAV2/9-CBA-FLEX-eGFP (A-D) or AAV2/9-hsyn-FLEX-eGFP (E-H) into the right striatum. GFP⁺ cells were present in the GP (E) and cortex (A). Co-localization (D,H) of native GFP fluorescence (B,F) with parvalbumin staining (C,G). (A, E) have been acquired with a Zeiss Axioscan Z.1 (Carl Zeiss Microscopy, Germany) using a 20x magnification and (B-D & F-H) have been acquired using Zeiss LSM 800 (Carl Zeiss Microscopy, Germany) with a 20x magnification.

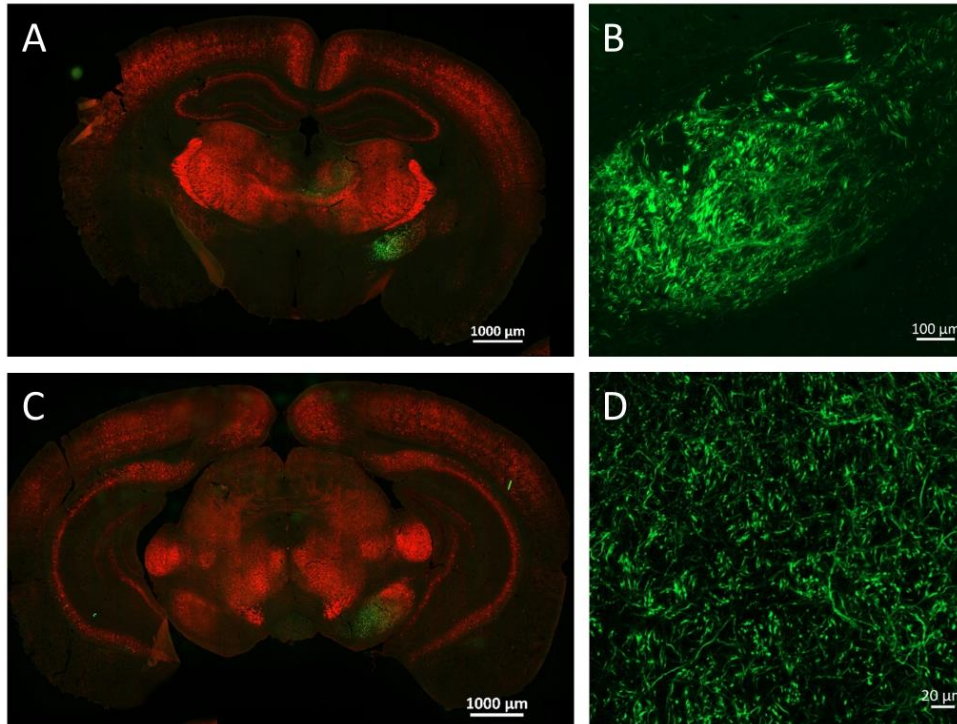
321

322 *Anterograde transport of GFP from GP PV⁺ neurons projecting to the SNr and STN*

323 GP contains 40% of PV⁺ neurons which project to the subthalamic nucleus (STN), to the
324 substantia nigra pars reticulata (SNr) or to the striatum (Saunders, Huang et al. 2016).

325 Consistently, in animals with GP transduction, GFP⁺ fibers were evidenced in the STN (Fig.

326 3 A & B) and in the SNr (Fig. 3 C & D).



327

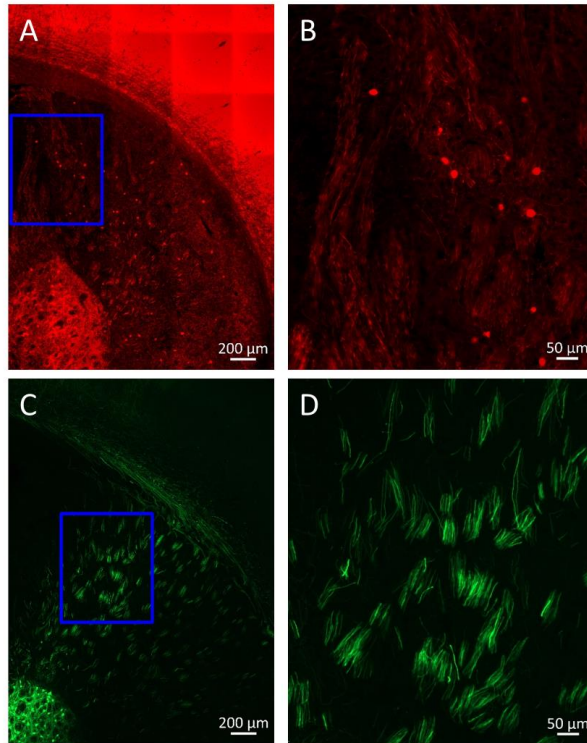
328 **Figure 3. Anterograde transport of GFP in fibers of GP PV⁺ neurons projecting to the**
 329 **subthalamic nucleus and to the substantia nigra pars reticulata.**

PV^{Cre} (+/+) mice were injected with AAV2/9-hsyn-FLEX-eGFP into the right striatum. In mice with a GP transduction, GFP⁺ fibers were detected in the subthalamic nucleus (STN) (A & B) and in the substantia nigra reticulata (SNr) (C & D). B and D, enlargement of the GFP⁺ area in the STN (A) and SNr (C), respectively.

330

331 In the striatum, it was not possible to distinguish GFP⁺ fibers originating from striatal
 332 interneurons and pallido-striatal projection neurons. A typical pattern of pallido-striatal fiber
 333 tracts was evidenced in WT mice by staining with an anti-PV antibody (Fig.4 A & B). In PV^{Cre}
 334 mice in which striatal AAV2/9 injection resulted in transduction of GP PV⁺ neurons, fiber
 335 tracts with the same pattern were GFP⁺(Fig.4 C & D), suggesting that, as expected they
 336 originate from the pallido-striatal projection neurons.

337



338

339 **Figure 4 Anterograde transport of GFP in fibers of GP PV⁺ neurons projecting to the striatum**

(A) PV staining (in red) of a wild-type non-injected mouse. (B) Dorsal striatum PV⁺ interneurons and fibers from pallidal PV⁺ projection neurons. (C) Mice with a massive GP transduction show pallido-striatal GFP⁺ fibers in the dorsal striatum (D). (B) Enlargement of the rectangle delineated in (A); (D) enlargement of the rectangle delineated in (C).

340

341 *Efficiency and cellular specificity of transgene expression in striatal PV⁺ interneurons*

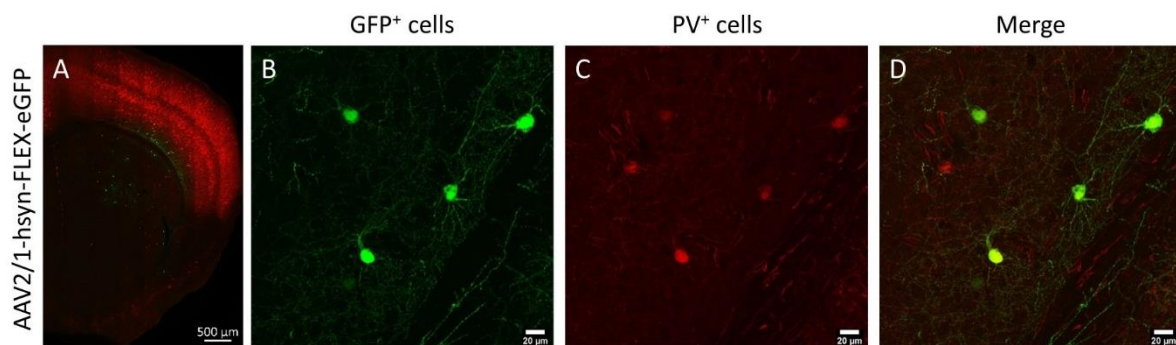
342 *mediated by AAV2/1-FLEX vectors in PV^{Cre} mice.*

343 Since AAV9 vectors diffusion to the GP and to the CTX hindered the selective targeting of
 344 the striatum, we used the AAV1 serotype which has previously been shown to allow region-
 345 targeted striatal transduction in rats (Burger, Gorbatyuk et al. 2004) (Bockstael, Chtarto et al.
 346 2008). In mice, however, a moderate number of GFP⁺ cells in the GP were reported after
 347 intra-striatal injection of AAV2/1 vectors (Taymans, Vandenberghe et al. 2007).

348 Furthermore, since the CBA promoter appeared stronger than the hsyn promoter (Fig.1), a
 349 higher level of GFP expression was obtained in cells distant from the injection site (e.g. note
 350 the prominent cortical transduction in Fig.1 A).

351 Therefore, the *hsyn* promoter was selected for further experiments. Several stereotaxic
352 coordinates were evaluated to avoid GP transduction. Anteroposterior coordinates varied
353 between +1.0 and +1.2 and dorsoventral coordinates between -2.75 and -3.0. The
354 mediolateral coordinates were set at -1.8. A total of 5 mice were tested. GP transduction
355 could be avoided only with the most anterior and dorsal coordinates (AP=+1.2; ML=-1.8;
356 DV=-2.75) (n=3) (Fig. 5A).

357 The efficiency of PV⁺ interneurons transduction, evaluated as the number of double-labeled
358 PV⁺/GFP⁺ cells (Fig. 5 D), relative to the total number of PV⁺ cells (Fig.5 C) was approx..
359 93%) (Table 2). The specificity of the targeting, evaluated as the number of double-labeled
360 PV⁺/GFP⁺ cells relative to the total number of GFP⁺ cells (Fig. 5 B), was higher than approx.
361 89% (Table 2). As for AAV9, injection into wild-type mice did not result in GFP⁺ cells.
362 In order to confirm on a larger number of animals that the established stereotaxic
363 coordinates (AP=+1.2; ML=-1.8; DV=-2.75) allow to avoid AAV1 viral particles diffusion to
364 the GP, 4 additional mice, taken from a different littermate of PV^{Cre} (+/+) mice, were injected
365 with AAV2/1-*hsyn*-FLEX-eGFP. However, in this littermate, the loss of PV⁺ cells in the
366 striatum was aggravated and only few PV⁺ and GFP⁺ cells were observed, precluding a
367 relevant statistical analysis (Suppl.Fig. 2A). However, despite an apparently normal amount
368 of PV⁺ cells in the GP, no GFP⁺ cells were observed (Suppl.Fig. 2B).



369

370 **Figure 5 Efficiency and specificity of AAV2/1-FLEX-*hsyn*-mediated PV⁺ striatal interneurons**
371 **transduction in PV^{Cre} (+/+) mice**

PV^{Cre} (+/+) mice were injected with AAV2/1-*hsyn*-FLEX-eGFP vectors. (A) Distribution of GFP⁺ cells in the striatum (Axioscan 20-fold). Confocal pictures showing co-localization (D) of native GFP fluorescence (B) with parvalbumin staining (C). Control wild-type mice injected with the same vectors did not harbor GFP⁺ cells (data not shown)

372

373 *Retrograde transduction of pallido-striatal neurons by AAV-FLEX vectors?*

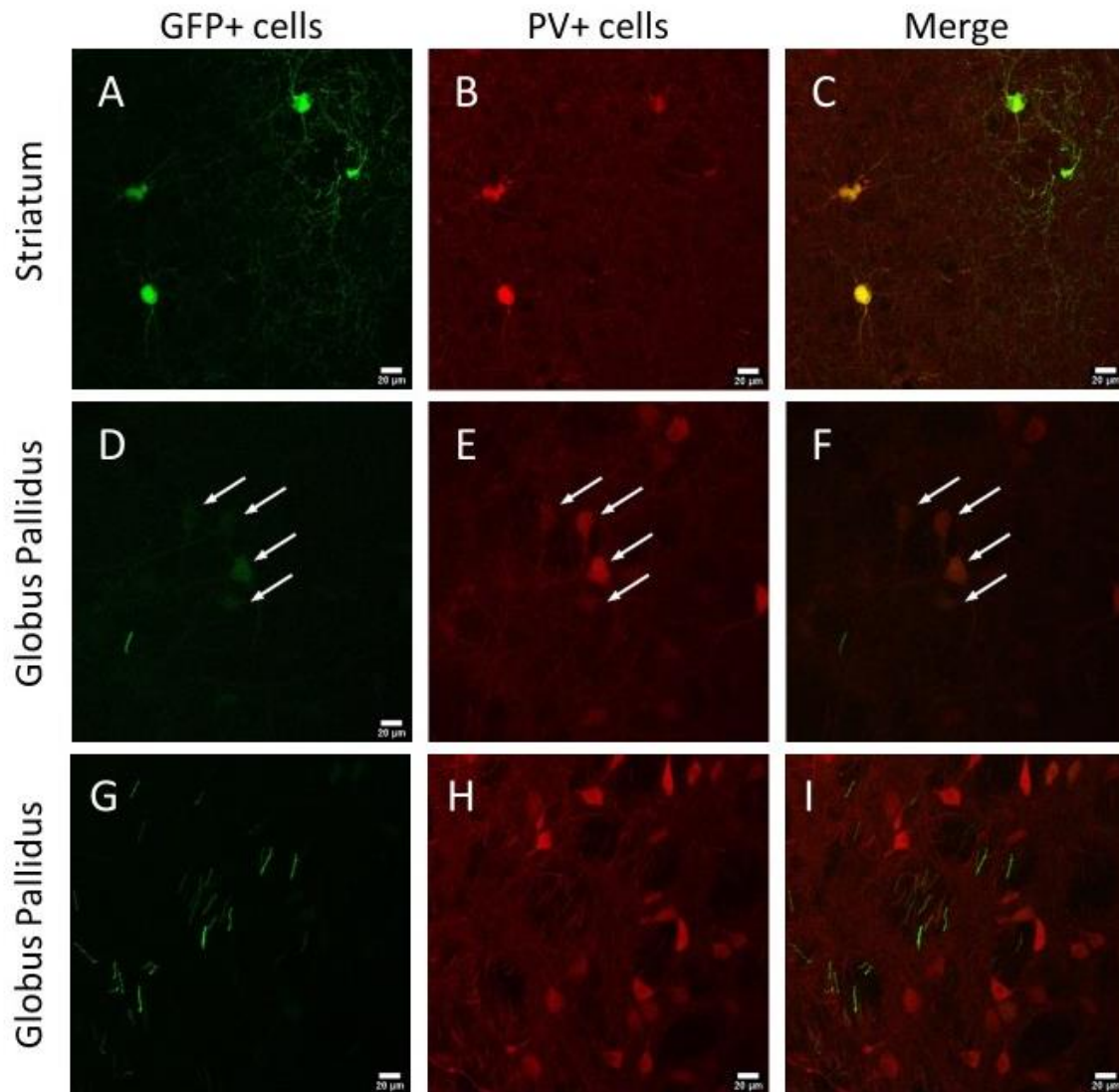
374 Since vectors were injected in the dorsolateral striatum in which pallido-striatal PV⁺ neurons
375 project, in the absence of diffusion, GP PV⁺ neurons could nevertheless be retrogradely
376 transduced.

377 Therefore, we examined the GP of 4 AAV2/9-hsyn and 3 AAV2/1-hsyn-injected mice
378 apparently devoided of direct GP transduction as shown in Fig. 2 E-H.

379 In one AAV2/9-injected mice, few GFP⁺ cells were observed in the GP (Fig. 6 D). As
380 expected these native GFP fluorescent cells were also PV⁺ (Fig. 6 E & F). However, the
381 level of fluorescence intensity of GFP⁺ cells in the GP was lower than the fluorescence of
382 directly transduced striatal cells (Fig.6 A), also labeled by anti-PV immunofluorescence
383 (Fig.6 B & C). Whether these GFP⁺ cells resulted from retrotransduction of pallido-striatal
384 projection neurons or residual diffusion of viral particles remains to be determined. The
385 mean fluorescence intensity of the GFP⁺ cells in the GP (n=4) was drastically lower than
386 striatal GFP⁺ cells in the same animal (n=4) , respectively 5.90 ± 3.69 and 76.98 ± 7.78 A.U.

387 In 2 other AAV2/9-injected mice, no GFP⁺ cells were detected in the GP but some fibers
388 were evidenced (Fig.6 G-I). The origin of these GFP⁺/PV⁺ fibers in the GP remains to be
389 determined. Finally, in the last AAV2/9-injected mice, no GFP⁺ cells or fibers were observed.
390 These data suggest that if AAV2/9 retrograde transduction of pallido-striatal neurons
391 occurred, it was very inefficient.

392 In AAV2/1-injected mice, devoided of direct GP transduction, no GFP⁺ cells were detected in
393 the GP (data not shown).



394

395 **Figure 6. Retrograde transduction of GP PV⁺ neurons mediated by AAV2/9-hsyn-FLEX-eGFP**
 396 **injected in the dorsal striatum?**

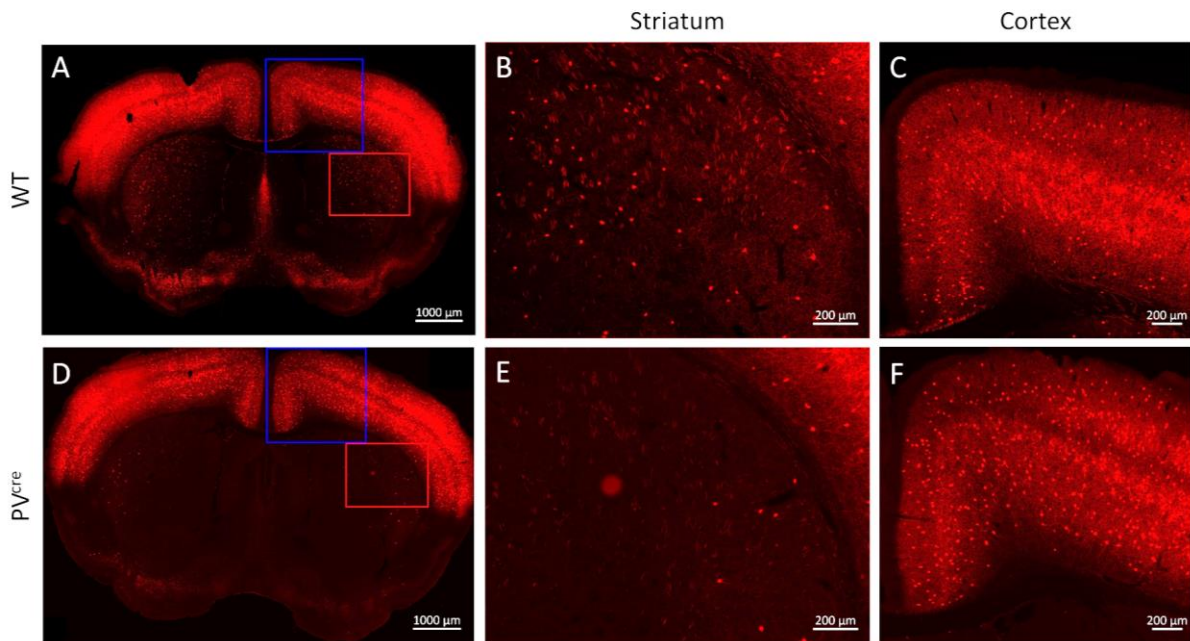
PV^{Cre} (+/+) mice were injected with AAV2/9-hsyn-FLEX-eGFP vector. Animals showing no efficient and widespread transduction (as shown in Fig.2 E-H) were further examined. (A-C) Transduced cells in the dorsal striatum. (D-F) Mice showing 4 GFP⁺ cells in the GP- (G-I) 1 out 2 mice showing GFP⁺ fibers in the GP.

397

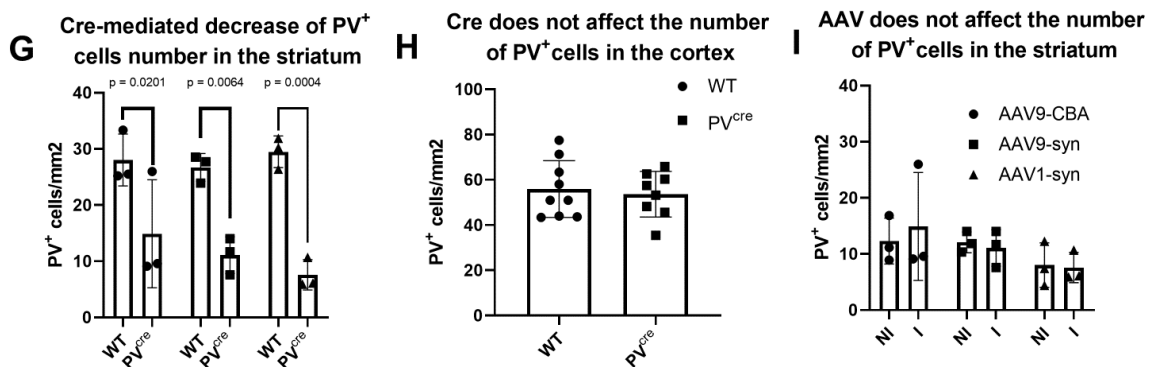
398 *Decrease of PV-expressing cells in the striatum of PV^{Cre} mice*

399 Continuous postnatal Cre expression has previously been reported to cause a decrease of
 400 cell numbers of some cell types such as immune cells (Schmidt-Supprian and Rajewsky
 401 2007) (Zeitrag, Alterauge et al. 2020) or retinal pigmented epithelium cells (He, Marioutina et
 402 al. 2014).

403 Therefore, we compared the number of PV⁺ cells in WT and PV^{Cre} homozygous mice.
 404 The number of PV⁺ cells was drastically (approx. 2-fold) reduced in the striatum (Fig. 7 G)
 405 but not in the CTX (Fig. 7 H) of PV^{Cre} mice as compared to WT mice (compare Fig. 7 A-C to
 406 Fig. 7 D-F).
 407 In order to determine whether Cre effect could be aggravated by viral transduction, injected
 408 and non-injected hemispheres of PV^{Cre} mice were compared for the 3 vectors (Fig. 7 I). No
 409 difference was observed. As a control, the number of PV⁺ cells in the left and right
 410 hemispheres of 3 non-injected WT mice were compared. No difference was observed
 411 (40.61±3.88 and 39.92±3.19 cells/mm² for the right and left hemispheres respectively;
 412 student t test: p=0.8240).



413



414

415 **Figure 7. Decrease of striatal PV⁺ cells in PV^{Cre} mice**

Wild-type (A-C) and PV^{Cre} (D-F) mice were injected with different AAV-FLEX vectors.

Cre decreases the number of PV⁺ cells in the striatum but not in the cortex. In the striatum (B & E), the number of PV⁺ cells was significantly reduced in PV^{Cre} mice (two-way ANOVA with Sidak's multiple comparison test; p=0.0201 for AAV2/9-CBA-FLEX-eGFP; p=0.0064 for AAV2/9-hsyn-FLEX-eGFP; p=0.0004 for AAV2/1-hsyn-FLEX-eGFP) (G). Circles, AAV2/9-CBA-FLEX-eGFP; squares, AAV2/9-hsyn-FLEX-eGFP; triangles, AAV2/1-hsyn-FLEX-eGFP. In the cortex (C & F), the number of PV⁺ cells in PV^{Cre} mice was not significantly different from the number of PV⁺ cells in WT mice (Student t test) (H). Circles, wild-type mice; squares, PV^{Cre} mice.

Viral toxicity The number of PV⁺ cells in the injected hemisphere of PV^{Cre} mice was compared to the contralateral non-injected hemisphere (I). Statistical analysis did not reveal a significant difference (two-way ANOVA with Sidak's multiple comparison test). Circles, AAV2/9-CBA-FLEX-eGFP; squares, AAV2/9-hsyn-FLEX-eGFP; triangles, AAV2/1-hsyn-FLEX-eGFP.

416

417

418 **Discussion**

419 In order to study the role of different types of neurons in complex neuronal circuits, it
420 is crucial to have available molecular tools allowing to selectively deliver genetic information
421 in targeted neuronal subpopulations. Furthermore, it is key to avoid transducing neurons with
422 similar functions in other brain regions which could perturb the behavioral and functional
423 outcomes. Thus, both cell type-specific and region-specific targeting are required.

424 In the present study, we focused on the targeting of transgene expression into mice
425 PV⁺ interneurons of the dorsal striatum. These interneurons, also called “fast-spiking”,
426 although representing a very small proportion of striatal neurons (approx. 0.5%), are key to
427 the coordination of striatal projections neurons which modulate the sensory-motor loop.

428 PV^{Cre} transgenic mice combined with Cre-dependent AAV vectors have been widely
429 used to target PV-expressing neurons in the cerebral cortex, hippocampus and thalamus
430 (Daigle, Madisen et al. 2018) (Madisen, Zwingman et al. 2010). However, very few studies
431 aimed at targeting striatal PV⁺ interneurons (Abreu, Gama et al. 2018, Enterria-Morales,
432 Lopez-Lopez et al. 2020).

433 In order to achieve efficient and selective transduction of striatal PV⁺ interneurons,
434 we compared 2 different AAV serotypes known to efficiently transduce the CNS, AAV2/1
435 (Burger, Gorbatyuk et al. 2004) (Bockstael, Chtarto et al. 2008) and AAV2/9 (Ciesielska,

436 Hadaczek et al. 2012) (Klein, Dayton et al. 2008), and 2 different transcription promoters, the
437 human synapsin (hsyn) and the hybrid chicken β -actin/CMV (CBA) promoters.

438 We show that, due to the diffusion of viral particles in the brain parenchyma, it is
439 difficult to target the dorsal striatum while avoiding diffusion to the GP. In contrast to the
440 sparse distribution of PV⁺ striatal interneurons, the GP contains a high density of PV⁺
441 neurons (40% of the total) which project to the STN, the SNr and the striatum (Saunders,
442 Huang et al. 2016). Transduction of PV⁺ GP projection neurons severely compromised the
443 targeting of PV⁺ striatal interneurons. Precise stereotaxic coordinates adjustment in the
444 dorsolateral striatum, AAV1 capsids (diffusing less than AAV9), and the hsyn promoter
445 (having a moderate transcriptional activity) were necessary to avoid direct transduction of
446 GP PV⁺ neurons. Such an extrastriatal PV⁺ neuronal transduction after striatal injections of
447 AAV-FLEX vectors, has been previously described and authors *a posteriori* excluded from
448 their behavioral analysis the animals showing a transduction in untargeted areas (Xu, Li et
449 al. 2016).

450 None of the vectors provided any GFP⁺ cell in WT mice demonstrating the tight Cre-
451 dependency of transgene expression. With all tested vectors, the proportion of GFP⁺ cells
452 stained by anti-PV antibodies was higher than 85%. However, GFP⁺ cells not expressing PV
453 at a detectable level were observed. This could be due to an effect of the Cre recombinase
454 towards PV⁺ neurons. Indeed, we observed that the number of PV⁺ cells was drastically
455 reduced (~ 2-fold) in the striatum of PV^{Cre} mice. This Cre-mediated effect was specific to
456 striatal PV⁺ neurons since no reduction of PV⁺ cells was observed in the cerebral cortex. A
457 similar phenomenon has been reported in retinal pigmented cells in which Cre expression
458 resulted in age- and dosage- dependent attenuation of β catenin and phalloidin stainings in
459 VDM2-Cre mice (He, Marioutina et al. 2014). It remains to be determined whereas Cre effect
460 on PV⁺ cells is also present in heterozygous Pvalbm1/Arbr mice. During the writing of this
461 manuscript, Enteria-Moralez and collaborators reported a similar effect of Cre towards PV⁺
462 cells in the striatum of homozygous Pvalbm1/Arbr mice. In this study, heterozygous Cre (+/-)

463 mice showed a non-significant decrease of PV mRNA. However, the small number of mice
464 (n=2 for some groups) precluded valid statistical analysis.

465 AAV vectors have previously been reported to have a toxic effect on specific classes
466 of neurons in particular when expressing GFP. Indeed, nigral injection of AAV2/1 vectors in
467 rats resulted in a decrease of the number of TH-expressing neurons, which was further
468 aggravated in the presence of GFP (Albert, Voutilainen et al. 2019). AAV2/9 vectors
469 expressing GFP were furthermore shown to elicit an inflammatory response in the rat
470 striatum (Samaranch, San Sebastian et al. 2014).

471 Another potential off-target effect could result from retrograde transport of AAV viral
472 particles in pallidostriatal fibers and transgene expression in GP PV⁺ projection neurons
473 (Saunders, Huang et al. 2016). AAV retrograde transport depends on the capsid serotype
474 and inconsistent data have been reported. For example, AAV1 retrograde transport has
475 been repeatedly found to be negligible (Burger, Gorbatyuk et al. 2004) (Bockstael, Chtarto et
476 al. 2008) (Oh, Harris et al. 2014) (Tervo, Hwang et al. 2016) although another report shows
477 that it occurred with a moderate efficiency in nigrostriatal dopaminergic neurons (Taymans,
478 Vandenberghe et al. 2007). Surprisingly, efficient retrograde infection was demonstrated with
479 AAV2/1-FLEX vectors in several types of neurons (Rothermel, Brunert et al. 2013) whereas,
480 in the same study, a constitutive AAV2/1 vector expressing mCherry from the CBA promoter
481 but not one expressing eGFP from the hsyn promoter, was proficient for retrograde
482 transduction. Similarly, inconsistent reports of AAV9 serotype retrograde transport efficiency
483 have been published (Klein, Dayton et al. 2008) (Tervo, Hwang et al. 2016) (Cearley and
484 Wolfe 2006) (Gallagher, Watson et al. 2008). In a comparative study, (Tervo, Hwang et al.
485 2016) AAV1 ability to undergo retrograde transport was found to be lower than that of AAV9.
486 Different species (rat versus mice), different neuronal pathways, expression levels driven by
487 the chosen promoter and titers of the vector may explain these discrepancies.
488 To our knowledge, retrograde transduction of GP PV⁺ neurons following intrastriatal AAV
489 injection has never been described. In our study, in the absence of apparent diffusion, only a
490 very low number of GFP⁺ cells were detected in 1 out of 4 AAV2/9-injected mice examined,

491 and their native green fluorescence was lower than at the target site in the striatum.
492 Furthermore, it cannot be excluded that the observed GFP⁺ cells in the GP resulted from a
493 low level of diffusion rather than retrograde transport. In contrast, with AAV2/1 vector, no
494 retrograde transduction of pallidostriatal neurons was observed in our conditions.

495 In conclusion, caution should be taken when interpreting functional and behavioral
496 data obtained in the PV^{Cre} mice/AAV-FLEX system. First, it is key to avoid transducing PV
497 neurons in other brain regions which will perturb the behavioral and functional outcomes. GP
498 PV⁺ neurons project to the STN, SNr and striatum (Saunders, Huang et al. 2016), nuclei
499 which are all involved in the motor loop. Thus, transduction of these neurons might
500 drastically modify the functional effects of transgene expression. Secondly, the herein
501 described Cre-mediated deleterious effect toward PV⁺ striatal interneurons could reflect
502 neuronal cell death or loss of PV expression. In the latter case, these neurons are probably
503 dysfunctional since PV, a calcium-binding protein is important for neuronal activity.
504 Perturbation of the synaptic plasticity of these fast-spiking neurons which are thought to
505 coordinate the activity of striatal projection neurons, might severely affect the motor loop. It
506 should be noted that, in a model of AAV-mediated Cre expression, neuronal programmed
507 cell death inducing behavioral perturbations were described (Rezai Amin, Gruszczynski et al.
508 2019)

509 In order to achieve targeted gene delivery into fast-spiking striatal interneurons
510 without the use of PV^{Cre} mice and AAV-Flex vectors, a more selective transcriptional
511 targeting could be designed. Viral vectors with specific enhancers allowing to target neuronal
512 or glial cell populations in wild-type animals are coming to an era (Dimidschstein, Chen et al.
513 2016) (Meunier, Merienne et al. 2016) (Pignataro, Sucunza et al. 2017) (Vormstein-
514 Schneider, Lin et al. 2020).

515

516 **Acknowledgements**

517 We thank Valentine Golzne for technical assistance.

518 We thank Jacques Barraud, Geraldine Rochat and Myriam Vuillet (Central animal house,
519 Lausanne University Hospital) for the breeding of PV^{Cre} mice.
520 Scanning and confocal imaging was performed in CIF Lausanne imaging platform. We thank
521 Luigi Bozzo and Florence Morgenthaler-Grand.
522 This work was supported by a grant from the Swiss National Foundation (SNF grant number
523 31003A_179527).
524 All authors declare that they have no conflict of interest.

525

526 **Authors contribution**

527 **Marcelo Duarte-Azevedo:** Conceptualization, Methodology, Validation, Formal analysis,

528 Investigation, Data curation, Writing-Review and editing, Visualization

529 **Sibilla Sander:** Conceptualization, Methodology, Validation, Formal analysis, Investigation, Data

530 curation, Writing-Review and editing, Visualization

531 **Cheryl Jeanneret:** Validation, Formal analysis, Investigation, Data curation, Writing-Review and

532 editing,

533 **Soophie Olfat:** Investigation

534 **Liliane Tenenbaum:** Conceptualization, Writing-original draft, Supervision, Project administration,

535 Funding acquisition.

536

537 Abreu, C. M., L. Gama, S. Krasemann, M. Chesnut, S. Odwin-Dacosta, H. T. Hogberg, T. Hartung
538 and D. Pamies (2018). "Microglia Increase Inflammatory Responses in iPSC-Derived Human
539 BrainSpheres." *Front Microbiol* **9**: 2766.

540 Albert, K., M. H. Voutilainen, A. Domanskyi, T. P. Piepponen, S. Ahola, R. K. Tuominen, C. Richie, B.
541 K. Harvey and M. Airavaara (2019). "Downregulation of tyrosine hydroxylase phenotype after AAV
542 injection above substantia nigra: Caution in experimental models of Parkinson's disease." *J Neurosci*
543 *Res* **97**(3): 346-361.

544 Aurnhammer, C., M. Haase, N. Muether, M. Hausl, C. Rauschhuber, I. Huber, H. Nitschko, U. Busch,
545 A. Sing, A. Ehrhardt and A. Baiker (2012). "Universal real-time PCR for the detection and
546 quantification of adeno-associated virus serotype 2-derived inverted terminal repeat sequences." *Hum*
547 *Gene Ther Methods* **23**(1): 18-28.

548 Bedbrook, C. N., B. E. Deverman and V. Gradinaru (2018). "Viral Strategies for Targeting the Central
549 and Peripheral Nervous Systems." *Annu Rev Neurosci* **41**: 323-348.

550 Bockstael, O., A. Chtarto, J. Wakkinen, X. Yang, C. Melas, M. Levivier, J. Brotchi and L. Tenenbaum
551 (2008). "Differential transgene expression profiles in rat brain, using rAAV2/1 vectors with tetracycline-
552 inducible and cytomegalovirus promoters." *Hum Gene Ther* **19**(11): 1293-1305.

553 Buenostro, J. D., B. Wu, U. M. Litzenburger, D. Ruff, M. L. Gonzales, M. P. Snyder, H. Y. Chang and
554 W. J. Greenleaf (2015). "Single-cell chromatin accessibility reveals principles of regulatory variation."
555 *Nature* **523**(7561): 486-490.

556 Burger, C., O. S. Gorbatyuk, M. J. Velardo, C. S. Peden, P. Williams, S. Zolotukhin, P. J. Reier, R. J.
557 Mandel and N. Muzyczka (2004). "Recombinant AAV viral vectors pseudotyped with viral capsids

558 from serotypes 1, 2, and 5 display differential efficiency and cell tropism after delivery to different
559 regions of the central nervous system." *Mol Ther* **10**(2): 302-317.

560 Casanova, F., P. R. Carney and M. Santinoranont (2014). "Effect of needle insertion speed on tissue
561 injury, stress, and backflow distribution for convection-enhanced delivery in the rat brain." *PLoS One*
562 **9**(4): e94919.

563 Castle, M. J., Z. T. Gershenson, A. R. Giles, E. L. Holzbaur and J. H. Wolfe (2014). "Adeno-
564 associated virus serotypes 1, 8, and 9 share conserved mechanisms for anterograde and retrograde
565 axonal transport." *Hum Gene Ther* **25**(8): 705-720.

566 Cearley, C. N. and J. H. Wolfe (2006). "Transduction characteristics of adeno-associated virus vectors
567 expressing cap serotypes 7, 8, 9, and Rh10 in the mouse brain." *Mol Ther* **13**(3): 528-537.

568 Chen, H., D. M. McCarty, A. T. Bruce and K. Suzuki (1999). "Oligodendrocyte-specific gene
569 expression in mouse brain: use of a myelin-forming cell type-specific promoter in an adeno-associated
570 virus." *J Neurosci Res* **55**(4): 504-513.

571 Chen, H., D. M. McCarty, A. T. Bruce, K. Suzuki and K. Suzuki (1998). "Gene transfer and expression
572 in oligodendrocytes under the control of myelin basic protein transcriptional control region mediated
573 by adeno-associated virus." *Gene Ther* **5**(1): 50-58.

574 Chtarto, A., O. Bockstael, T. Tshibangu, O. Dewitte, M. Levivier and L. Tenenbaum (2013). "A next
575 step in adeno-associated virus-mediated gene therapy for neurological diseases: regulation and
576 targeting." *Br J Clin Pharmacol* **76**(2): 217-232.

577 Ciesielska, A., P. Hadaczek, G. Mittermeyer, S. Zhou, J. F. Wright, K. S. Bankiewicz and J. Forsayeth
578 (2013). "Cerebral Infusion of AAV9 Vector-encoding Non-self Proteins Can Elicit Cell-mediated
579 Immune Responses." *Mol Ther*. **21**(1), 158–166.

580 Daigle, T. L., L. Madisen, T. A. Hage, M. T. Valley, U. Knoblich, R. S. Larsen, M. M. Takeno, L.
581 Huang, H. Gu, R. Larsen, M. Mills, A. Bosma-Moody, L. A. Siverts, M. Walker, L. T. Graybuck, Z. Yao,
582 O. Fong, T. N. Nguyen, E. Garren, G. H. Lenz, M. Chavarha, J. Pendergraft, J. Harrington, K. E.
583 Hirokawa, J. A. Harris, P. R. Nicovich, M. J. McGraw, D. R. Ollerenshaw, K. A. Smith, C. A. Baker, J.
584 T. Ting, S. M. Sunkin, J. Lecoq, M. Z. Lin, E. S. Boyden, G. J. Murphy, N. M. da Costa, J. Waters, L.
585 Li, B. Tasic and H. Zeng (2018). "A Suite of Transgenic Driver and Reporter Mouse Lines with
586 Enhanced Brain-Cell-Type Targeting and Functionality." *Cell* **174**(2): 465-480 e422.

587 Dalkara, D., L. C. Byrne, R. R. Klimczak, M. Visel, L. Yin, W. H. Merigan, J. G. Flannery and D. V.
588 Schaffer (2013). "In vivo-directed evolution of a new adeno-associated virus for therapeutic outer
589 retinal gene delivery from the vitreous." *Sci Transl Med* **5**(189): 189ra176.

590 Dashkoff, J., E. P. Lerner, N. Truong, J. A. Klickstein, Z. Fan, D. Mu, C. A. Maguire, B. T. Hyman and
591 E. Hudry (2016). "Tailored transgene expression to specific cell types in the central nervous system
592 after peripheral injection with AAV9." *Mol Ther Methods Clin Dev* **3**: 16081.

593 Dimidschstein, J., Q. Chen, R. Tremblay, S. L. Rogers, G. A. Saldi, L. Guo, Q. Xu, R. Liu, C. Lu, J.
594 Chu, J. S. Grimley, A. R. Krostag, A. Kaykas, M. C. Avery, M. S. Rashid, M. Baek, A. L. Jacob, G. B.
595 Smith, D. E. Wilson, G. Kosche, I. Kruglikov, T. Rusielewicz, V. C. Kotak, T. M. Mowery, S. A.
596 Anderson, E. M. Callaway, J. S. Dasen, D. Fitzpatrick, V. Fossati, M. A. Long, S. Noggle, J. H.
597 Reynolds, D. H. Sanes, B. Rudy, G. Feng and G. Fishell (2016). "A viral strategy for targeting and
598 manipulating interneurons across vertebrate species." *Nat Neurosci* **19**(12): 1743-1749.

599 Dirren, E., C. L. Towne, V. Setola, D. E. Redmond, Jr., B. L. Schneider and P. Aebischer (2014).
600 "Intracerebroventricular injection of adeno-associated virus 6 and 9 vectors for cell type-specific
601 transgene expression in the spinal cord." *Hum Gene Ther* **25**(2): 109-120.

602 Drinkut, A., Y. Tereshchenko, J. B. Schulz, M. Bahr and S. Kugler (2012). "Efficient gene therapy for
603 Parkinson's disease using astrocytes as hosts for localized neurotrophic factor delivery." *Mol Ther*
604 **20**(3): 534-543.

605 Enterría-Morales, D., I. Lopez-Lopez, J. Lopez-Barneo and X. d'Anglemont de Tassigny (2020). "Role
606 of glial cell line-derived neurotrophic factor in the maintenance of adult mesencephalic
607 catecholaminergic neurons." *Mov Disord*.

608 Fischer, K. B., H. K. Collins and E. M. Callaway (2019). "Sources of off-target expression from
609 recombinase-dependent AAV vectors and mitigation with cross-over insensitive ATG-out vectors."
610 *Proc Natl Acad Sci U S A*. **116**(52), 27001–27010.

611 Gallagher, P., S. Watson, C. Elizabeth Dye, A. H. Young and I. Nicol Ferrier (2008). "Persistent
612 effects of mifepristone (RU-486) on cortisol levels in bipolar disorder and schizophrenia." *J Psychiatr*
613 *Res* **42**(12): 1037-1041.

614 Geiger, J. R., T. Melcher, D. S. Koh, B. Sakmann, P. H. Seeburg, P. Jonas and H. Monyer (1995).
615 "Relative abundance of subunit mRNAs determines gating and Ca²⁺ permeability of AMPA receptors
616 in principal neurons and interneurons in rat CNS." *Neuron* **15**(1): 193-204.

617 Gokce, O., G. M. Stanley, B. Treutlein, N. F. Neff, J. G. Camp, R. C. Malenka, P. E. Rothwell, M. V.
618 Fuccillo, T. C. Sudhof and S. R. Quake (2016). "Cellular Taxonomy of the Mouse Striatum as
619 Revealed by Single-Cell RNA-Seq." Cell Rep **16**(4): 1126-1137.

620 Grames, M. S., R. D. Dayton, K. L. Jackson, A. D. Richard, X. Lu and R. L. Klein (2018). "Cre-
621 dependent AAV vectors for highly targeted expression of disease-related proteins and
622 neurodegeneration in the substantia nigra." FASEB J **32**(8): 4420-4427.

623 Gritton, H. J., W. M. Howe, M. F. Romano, A. G. DiFeliceantonio, M. A. Kramer, V. Saligrama, M. E.
624 Bucklin, D. Zemel and X. Han (2019). "Unique contributions of parvalbumin and cholinergic
625 interneurons in organizing striatal networks during movement." Nat Neurosci **22**(4): 586-597.

626 Hadaczek, P., Y. Yamashita, H. Mirek, L. Tamas, M. C. Bohn, C. Noble, J. W. Park and K. Bankiewicz
627 (2006). "The "perivascular pump" driven by arterial pulsation is a powerful mechanism for the
628 distribution of therapeutic molecules within the brain." Mol Ther **14**(1): 69-78.

629 Hartmann, J., F. B. Thalheimer, F. Hopfner, T. Kerzel, K. Khodosevich, D. Garcia-Gonzalez, H.
630 Monyer, I. Diester, H. Buning, J. E. Carette, P. Fries and C. J. Buchholz (2019). "GluA4-Targeted AAV
631 Vectors Deliver Genes Selectively to Interneurons while Relying on the AAV Receptor for Entry." Mol
632 Ther Methods Clin Dev **14**: 252-260.

633 He, L., M. Marioutina, J. L. Dunaief and A. G. Marneros (2014). "Age- and gene-dosage-dependent
634 cre-induced abnormalities in the retinal pigment epithelium." Am J Pathol **184**(6): 1660-1667.

635 Hippenmeyer, S., E. Vrieseling, M. Sigrist, T. Portmann, C. Laengle, D. R. Ladle and S. Arber (2005).
636 "A developmental switch in the response of DRG neurons to ETS transcription factor signaling." PLoS
637 Biol **3**(5): e159.

638 Hocquemiller, M., L. Giersch, M. Audrain, S. Parker and N. Cartier (2016). "Adeno-Associated Virus-
639 Based Gene Therapy for CNS Diseases." Hum Gene Ther **27**(7): 478-496.

640 Hunnicutt, B. J., B. C. Jongbloets, W. T. Birdsong, K. J. Gertz, H. Zhong and T. Mao (2016). "A
641 comprehensive excitatory input map of the striatum reveals novel functional organization." Elife **5**.

642 Jolle, C., N. Deglon, C. Pythoud, A. K. Bouzier-Sore and L. Pellerin (2019). "Development of Efficient
643 AAV2/DJ-Based Viral Vectors to Selectively Downregulate the Expression of Neuronal or Astrocytic
644 Target Proteins in the Rat Central Nervous System." Front Mol Neurosci **12**: 201.

645 Juttner, J., A. Szabo, B. Gross-Scherf, R. K. Morikawa, S. B. Rompani, P. Hantz, T. Szikra, F.
646 Esposti, C. S. Cowan, A. Bharioke, C. P. Patino-Alvarez, O. Keles, A. Kusnyerik, T. Azoulay, D. Hartl,
647 A. R. Krebs, D. Schubeler, R. I. Hajdu, A. Lukats, J. Nemeth, Z. Z. Nagy, K. C. Wu, R. H. Wu, L.
648 Xiang, X. L. Fang, Z. B. Jin, D. Goldblum, P. W. Hasler, H. P. N. Scholl, J. Krol and B. Roska (2019).
649 "Targeting neuronal and glial cell types with synthetic promoter AAVs in mice, non-human primates
650 and humans." Nat Neurosci **22**(8): 1345-1356.

651 Kantor, B., T. McCown, P. Leone and S. J. Gray (2014). "Clinical applications involving CNS gene
652 transfer." Adv Genet **87**: 71-124.

653 Kim, Y., T. Kim, J. K. Rhee, D. Lee, K. Tanaka-Yamamoto and Y. Yamamoto (2015). "Selective
654 transgene expression in cerebellar Purkinje cells and granule cells using adeno-associated viruses
655 together with specific promoters." Brain Res **1620**: 1-16.

656 Klein, R. L., R. D. Dayton, J. B. Tatom, K. M. Henderson and P. P. Henning (2008). "AAV8, 9, Rh10,
657 Rh43 vector gene transfer in the rat brain: effects of serotype, promoter and purification method." Mol
658 Ther **16**(1): 89-96.

659 Klein, R. L., M. E. Hamby, Y. Gong, A. C. Hirko, S. Wang, J. A. Hughes, M. A. King and E. M. Meyer
660 (2002). "Dose and promoter effects of adeno-associated viral vector for green fluorescent protein
661 expression in the rat brain." Exp Neurol **176**(1): 66-74.

662 Klein, R. L., E. M. Meyer, A. L. Peel, S. Zolotukhin, C. Meyers, N. Muzyczka and M. A. King (1998).
663 "Neuron-specific transduction in the rat septohippocampal or nigrostriatal pathway by recombinant
664 adeno-associated virus vectors." Exp Neurol **150**(2): 183-194.

665 Korbelin, J., G. Dogbevia, S. Michelfelder, D. A. Ridder, A. Hunger, J. Wenzel, H. Seismann, M.
666 Lampe, J. Bannach, M. Pasparakis, J. A. Kleinschmidt, M. Schwaninger and M. Trepel (2016). "A
667 brain microvasculature endothelial cell-specific viral vector with the potential to treat neurovascular
668 and neurological diseases." EMBO Mol Med **8**(6): 609-625.

669 Kugler, S., P. Lingor, U. Scholl, S. Zolotukhin and M. Bahr (2003). "Differential transgene expression
670 in brain cells in vivo and in vitro from AAV-2 vectors with small transcriptional control units." Virology
671 **311**(1): 89-95.

672 Lee, A. T., D. Vogt, J. L. Rubenstein and V. S. Sohal (2014). "A class of GABAergic neurons in the
673 prefrontal cortex sends long-range projections to the nucleus accumbens and elicits acute avoidance
674 behavior." J Neurosci **34**(35): 11519-11525.

675 Lee, K., S. M. Holley, J. L. Shobe, N. C. Chong, C. Cepeda, M. S. Levine and S. C. Masmanidis
676 (2017). "Parvalbumin Interneurons Modulate Striatal Output and Enhance Performance during
677 Associative Learning." Neuron **93**(6): 1451-1463 e1454.

678 Liu, Z., A. Brown, D. Fisher, Y. Wu, J. Warren and X. Cui (2016). "Tissue Specific Expression of Cre
679 in Rat Tyrosine Hydroxylase and Dopamine Active Transporter-Positive Neurons." PLoS One **11**(2):
680 e0149379.

681 Lueshen, E., K. Tangen, A. I. Mehta and A. Linninger (2017). "Backflow-free catheters for efficient and
682 safe convection-enhanced delivery of therapeutics." Med Eng Phys **45**: 15-24.

683 Madisen, L., T. A. Zwingman, S. M. Sunkin, S. W. Oh, H. A. Zariwala, H. Gu, L. L. Ng, R. D. Palmiter,
684 M. J. Hawrylycz, A. R. Jones, E. S. Lein and H. Zeng (2010). "A robust and high-throughput Cre
685 reporting and characterization system for the whole mouse brain." Nat Neurosci **13**(1): 133-140.

686 Meunier, C., N. Merienne, C. Jolle, N. Deglon and L. Pellerin (2016). "Astrocytes are key but indirect
687 contributors to the development of the symptomatology and pathophysiology of Huntington's disease."
688 Glia **64**(11): 1841-1856.

689 Munoz-Manchado, A. B., C. Bengtsson Gonzales, A. Zeisel, H. Munguba, B. Bekkouche, N. G.
690 Skene, P. Lonnerberg, J. Ryge, K. D. Harris, S. Linnarsson and J. Hjerling-Leffler (2018). "Diversity of
691 Interneurons in the Dorsal Striatum Revealed by Single-Cell RNA Sequencing and PatchSeq." Cell
692 Rep **24**(8): 2179-2190 e2177.

693 Nieuwenhuis, B., B. Haenzi, S. Hilton, A. Carnicer-Lombarte, B. Hobo, J. Verhaagen and J. W.
694 Fawcett (2020). "Optimization of adeno-associated viral vector-mediated transduction of the
695 corticospinal tract: comparison of four promoters." Gene Ther.

696 Oh, S. W., J. A. Harris, L. Ng, B. Winslow, N. Cain, S. Mihalas, Q. Wang, C. Lau, L. Kuan, A. M.
697 Henry, M. T. Mortrud, B. Ouellette, T. N. Nguyen, S. A. Sorensen, C. R. Slaughterbeck, W. Wakeman,
698 Y. Li, D. Feng, A. Ho, E. Nicholas, K. E. Hirokawa, P. Bohn, K. M. Joines, H. Peng, M. J. Hawrylycz,
699 J. W. Phillips, J. G. Hohmann, P. Wohnoutka, C. R. Gerfen, C. Koch, A. Bernard, C. Dang, A. R.
700 Jones and H. Zeng (2014). "A mesoscale connectome of the mouse brain." Nature **508**(7495): 207-
701 214.

702 Pignataro, D., D. Sucunza, L. Vanrell, E. Lopez-Franco, I. G. Dopeso-Reyes, A. Vales, M. Hommel, A.
703 J. Rico, J. L. Lanciego and G. Gonzalez-Aseguinolaza (2017). "Adeno-Associated Viral Vectors
704 Serotype 8 for Cell-Specific Delivery of Therapeutic Genes in the Central Nervous System." Front
705 Neuroanat **11**: 2.

706 Rezai Amin, S., C. Gruszczynski, B. P. Guiard, J. Callebort, J. M. Launay, F. Louis, C. Betancur, V.
707 Vialou and S. Gautron (2019). "Viral vector-mediated Cre recombinase expression in substantia nigra
708 induces lesions of the nigrostriatal pathway associated with perturbations of dopamine-related
709 behaviors and hallmarks of programmed cell death." J Neurochem **150**(3): 330-340.

710 Rosario, A. M., P. E. Cruz, C. Ceballos-Diaz, M. R. Strickland, Z. Siemienski, M. Pardo, K. L. Schob,
711 A. Li, G. V. Aslanidi, A. Srivastava, T. E. Golde and P. Chakrabarty (2016). "Microglia-specific
712 targeting by novel capsid-modified AAV6 vectors." Mol Ther Methods Clin Dev **3**: 16026.

713 Rothermel, M., D. Brunert, C. Zabawa, M. Diaz-Quesada and M. Wachowiak (2013). "Transgene
714 expression in target-defined neuron populations mediated by retrograde infection with adeno-
715 associated viral vectors." J Neurosci **33**(38): 15195-15206.

716 Samaranch, L., W. San Sebastian, A. P. Kells, E. A. Salegio, G. Heller, J. R. Bringas, P. Pivrotto, S.
717 DeArmond, J. Forsayeth and K. S. Bankiewicz (2014). "AAV9-mediated expression of a non-self
718 protein in nonhuman primate central nervous system triggers widespread neuroinflammation driven by
719 antigen-presenting cell transduction." Mol Ther **22**(2): 329-337.

720 Saunders, A., K. W. Huang and B. L. Sabatini (2016). "Globus Pallidus Externus Neurons Expressing
721 parvalbumin Interconnect the Subthalamic Nucleus and Striatal Interneurons." PLoS One **11**(2):
722 e0149798.

723 Saunders, A., C. A. Johnson and B. L. Sabatini (2012). "Novel recombinant adeno-associated viruses
724 for Cre activated and inactivated transgene expression in neurons." Front Neural Circuits **6**: 47.

725 Saunders, A. and B. L. Sabatini (2015). "Cre Activated and Inactivated Recombinant Adeno-
726 Associated Viral Vectors for Neuronal Anatomical Tracing or Activity Manipulation." Curr Protoc
727 Neurosci **72**: 1 24 21-15.

728 Schmidt-Supprian, M. and K. Rajewsky (2007). "Vagaries of conditional gene targeting." Nat Immunol
729 **8**(7): 665-668.

730 Shevtsova, Z., J. M. Malik, U. Michel, M. Bahr and S. Kugler (2005). "Promoters and serotypes:
731 targeting of adeno-associated virus vectors for gene transfer in the rat central nervous system in vitro
732 and in vivo." Exp Physiol **90**(1): 53-59.

733 Stauffer, W. R., A. Lak, A. Yang, M. Borel, O. Paulsen, E. S. Boyden and W. Schultz (2016).
734 "Dopamine Neuron-Specific Optogenetic Stimulation in Rhesus Macaques." Cell **166**(6): 1564-1571
735 e1566.

736 Surmeier, D. J., J. Ding, M. Day, Z. Wang and W. Shen (2007). "D1 and D2 dopamine-receptor
737 modulation of striatal glutamatergic signaling in striatal medium spiny neurons." Trends Neurosci
738 **30**(5): 228-235.

739 Taymans, J. M., L. H. Vandenberghe, C. V. Haute, I. Thiry, C. M. Deroose, L. Mortelmans, J. M.
740 Wilson, Z. Debyser and V. Baekelandt (2007). "Comparative analysis of adeno-associated viral vector
741 serotypes 1, 2, 5, 7, and 8 in mouse brain." Hum Gene Ther **18**(3): 195-206.

742 Tenenbaum, L., F. Jurysta, A. Stathopoulos, Z. Puschban, C. Melas, W. T. Hermens, J. Verhaagen,
743 B. Pichon, T. Velu and M. Levivier (2000). "Tropism of AAV-2 vectors for neurons of the globus
744 pallidus." Neuroreport **11**(10): 2277-2283.

745 Tervo, D. G., B. Y. Hwang, S. Viswanathan, T. Gaj, M. Lavzin, K. D. Ritola, S. Lindo, S. Michael, E.
746 Kuleshova, D. Ojala, C. C. Huang, C. R. Gerfen, J. Schiller, J. T. Dudman, A. W. Hantman, L. L.
747 Looger, D. V. Schaffer and A. Y. Karpova (2016). "A Designer AAV Variant Permits Efficient
748 Retrograde Access to Projection Neurons." Neuron **92**(2): 372-382.

749 Vazquez, L. C., E. Hagel, B. J. Willenberg, W. Dai, F. Casanova, C. D. Batich and M. Sarntinoranont
750 (2012). "Polymer-coated cannulas for the reduction of backflow during intraparenchymal infusions." J
751 Mater Sci Mater Med **23**(8): 2037-2046.

752 Vormstein-Schneider, D., J. D. Lin, K. A. Pelkey, R. Chittajallu, B. Guo, M. A. Arias-Garcia, K.
753 Allaway, S. Sakopoulos, G. Schneider, O. Stevenson, J. Vergara, J. Sharma, Q. Zhang, T. P.
754 Franken, J. Smith, L. A. Ibrahim, M. A. KJ, E. Sabri, S. Huang, E. Favuzzi, T. Burbridge, Q. Xu, L.
755 Guo, I. Vogel, V. Sanchez, G. A. Saldi, B. L. Gorissen, X. Yuan, K. A. Zaghoul, O. Devinsky, B. L.
756 Sabatini, R. Batista-Brito, J. Reynolds, G. Feng, Z. Fu, C. J. McBain, G. Fishell and J. Dimidschstein
757 (2020). "Viral manipulation of functionally distinct interneurons in mice, non-human primates and
758 humans." Nat Neurosci. 23(12). 1629-1636..

759 Watakabe, A., M. Ohtsuka, M. Kinoshita, M. Takaji, K. Isa, H. Mizukami, K. Ozawa, T. Isa and T.
760 Yamamori (2015). "Comparative analyses of adeno-associated viral vector serotypes 1, 2, 5, 8 and 9
761 in marmoset, mouse and macaque cerebral cortex." Neurosci Res **93**: 144-157.

762 Woloszynowska-Fraser, M. U., P. Wulff and G. Riedel (2017). "Parvalbumin-containing GABA cells
763 and schizophrenia: experimental model based on targeted gene delivery through adeno-associated
764 viruses." Behav Pharmacol **28**(8): 630-641.

765 Xu, M., L. Li and C. Pittenger (2016). "Ablation of fast-spiking interneurons in the dorsal striatum,
766 recapitulating abnormalities seen post-mortem in Tourette syndrome, produces anxiety and elevated
767 grooming." Neuroscience **324**: 321-329.

768 Zeitrag, J., D. Alterauge, F. Dahlstrom and D. Baumjohann (2020). "Gene dose matters:
769 Considerations for the use of inducible CD4-CreER(T2) mouse lines." Eur J Immunol **50**(4): 603-605.

770 Zingg, B., X. L. Chou, Z. G. Zhang, L. Mesik, F. Liang, H. W. Tao and L. I. Zhang (2017). "AAV-
771 Mediated Anterograde Transsynaptic Tagging: Mapping Corticocollicular Input-Defined Neural
772 Pathways for Defense Behaviors." Neuron **93**(1): 33-47.

773 Zolotukhin, S., M. Potter, I. Zolotukhin, Y. Sakai, S. Loiler, T. J. Fraitas, Jr., V. A. Chiodo, T.
774 Phillipsberg, N. Muzyczka, W. W. Hauswirth, T. R. Flotte, B. J. Byrne and R. O. Snyder (2002).
775 "Production and purification of serotype 1, 2, and 5 recombinant adeno-associated viral vectors."
776 Methods **28**(2): 158-167.

777